9-20-2012

Precision Measurement of the 6He Half-Life and the Weak Axial Current in Nuclei

A. Knecht
University of Washington

R. Hong
University of Washington

D. W. Zumwalt
University of Washington

B. G. Delbridge
University of Washington

A. García
University of Washington

See next page for additional authors

PHYSICAL REVIEW C **86**, 035506 (2012)

Precision measurement of the ^{6}He half-life and the weak axial current in nuclei

A. Knecht,[1,*] R. Hong,[1] D. W. Zumwalt,[1] B. G. Delbridge,[1] A. García,[1] P. Müller,[2] H. E. Swanson,[1] I. S. Towner,[3] S. Utsuno,[1] W. Williams,[2,†] and C. Wrede[1,‡]

[1]*Department of Physics and Center for Experimental Nuclear Physics and Astrophysics, University of Washington, Seattle, Washington 98195, USA*

[2]*Physics Division, Argonne National Laboratory, Argonne, Illinois 60439, USA*

[3]*Cyclotron Institute, Texas A&M University, College Station, Texas 77843, USA*

(Received 15 June 2012; published 20 September 2012)

Background: The β decays of ^{3}H and ^{6}He can play an important role in testing nuclear wave-function calculations and fixing low-energy constants in effective-field theory approaches. However, there exists a large discrepancy between previous measurements of the ^{6}He half-life.

Purpose: Our measurement aims at resolving this long-standing discrepancy in the ^{6}He half-life and providing a reliable ft value and Gamow-Teller matrix element for comparison with theoretical *ab initio* calculations.

Method: We measured the ^{6}He half-life by counting the β-decay electrons with two scintillator detectors operating in coincidence.

Results: The measured ^{6}He half-life is $806.89 \pm 0.11_{\text{stat}}{}^{+0.23}_{-0.19\text{syst}}$ ms corresponding to a relative precision of 3×10^{-4}. Calculating the statistical rate function we determined the ft value to be $803.04^{+0.26}_{-0.23}$ s.

Conclusions: Our result resolves the previous discrepancy by providing a higher-precision result with careful analysis of potential systematic uncertainties. The result provides a reliable basis for future precision comparisons with *ab initio* calculations.

DOI: 10.1103/PhysRevC.86.035506 PACS number(s): 23.40.−s, 27.20.+n

I. INTRODUCTION

Precision measurements of electroweak processes in light nuclei can provide important tests of our understanding of electroweak interactions in the nuclear medium. Many interesting problems—ranging from solar fusion to neutrino interactions and muon and pion capture processes—depend on their correct modeling and calculation [1]. Recent progress in numerical techniques enables precise, *ab initio* calculations of wave functions for light nuclei starting with the nucleon-nucleon interaction and without assuming a frozen core of inactive particles [2–4].

The allowed weak nuclear decays driven by the axial current—called Gamow-Teller decays—have historically played an important role in testing wave functions because the main operator has a simple spin and isospin structure and does not possess any radial component. Systematic comparisons using shell-model wave functions showed that in order to reproduce observations the value for the weak axial coupling constant, g_A, had to be "quenched." For the sd-shell nuclei this difference amounted to about 30% with respect to that measured in free neutron decay [5,6]. In addition, when charge-exchange reactions were used to explore a large fraction of the Gamow-Teller strength sum rule, evidence also pointed to "quenching of the Gamow-Teller strength" [7,8]. However, the origin of the quenching is not completely clear. References [7,9,10] showed that, as shell-model calculations are allowed to introduce higher and higher excitations, the need to renormalize operators disappears. But it has also been pointed out that meson-exchange currents (mediating, for example, nucleon-delta excitations) could be responsible for at least some of the apparent quenching of strength [11,12].

The decays of ^{3}H and of ^{6}He are special because these systems are light enough that the corresponding *ab initio* calculations can be performed with precision. In particular, Refs. [4,13] and later [14,15] have shown that, using the case of ^{3}H to fix nucleon-delta excitations, the ft value for ^{6}He can be calculated to within a few percent. These two decays, then, can play an important role in testing the accuracy of nuclear wave-function calculations [4,13,14] or, as suggested in Ref. [15], in fixing low-energy constants in effective-field-theory calculations [1].

In this paper we present a more detailed description of the high-precision experimental determination of the half-life and ft value for ^{6}He published in Ref. [16]. Except for a small branch of $\sim 10^{-6}$ [17] the β decay of ^{6}He proceeds 100% to the ground state of ^{6}Li with an end point of 3.5 MeV. The ^{6}He half-life was previously determined by several works compiled in Table I and shown in Fig. 1.

As can be seen, the values spread over a range much wider than expected from the claimed uncertainties, which makes the currently reported average and precision of 806.7 ± 1.5 ms [36] unreliable. Averaging the five values shown in the inset in Fig. 1 with uncertainties below 1% and scaling the uncertainty by the square root of the χ^2 per degrees of freedom (DOF)—as advised by the Particle Data Group in

*knechta@uw.edu

†Present address: Department of Physics, Old Dominion University, Norfolk, VA 23529, USA.

‡Present address: Department of Physics and Astronomy and National Superconducting Cyclotron Laboratory, Michigan State University, East Lansing, MI 48824, USA.

TABLE I. Compilation of all previously obtained ^{6}He half-life values.

Year	Half-life (ms)	Ref.	Year	Half-life (ms)	Ref.
1946	850 ± 50	[18]	1956	852 ± 16	[19]
1947	870 ± 60	[20]	1958	830 ± 20	[21]
1948	820 ± 60	[22]	1962	797 ± 3	[23]
1949	823 ± 13	[24]	1962	862 ± 17	[25]
1952	860 ± 30	[26]	1963	830 ± 20	[27]
1952	840 ± 30	[28]	1974	808.1 ± 2.0	[29]
1953	830 ± 30	[30]	1981	798.1 ± 1.0	[31]
1954	799 ± 3	[32]	1982	805.4 ± 2.0	[33]
1955	850 ± 30	[34]	2002	810 ± 8	[35]

such cases [37]—results in 800.6 ± 2.0 ms. As emphasized by the author of the last precision measurement in 1982 [33], this needs to be resolved by improved and higher-precision experiments.

II. EXPERIMENTAL SETUP

We produced ^{6}He using the tandem Van de Graaff accelerator available at the Center for Experimental Nuclear Physics and Astrophysics of the University of Washington. A deuteron beam impinged on molten lithium held in a stainless steel cup, producing ^{6}He via the reaction ^{7}Li(^{2}H,^{3}He)^{6}He. The ^{6}He atoms subsequently diffused out into vacuum. A detailed description of the ^{6}He source, which can deliver more than 10^9 atoms/s to experiments, can be found in Ref. [38]. The ^{6}He atoms were transferred from the source through a turbomolecular pump to a low-background experimental area. The measuring volume consisted of a 35-mm-diam, 381-mm-long tube made of stainless steel sealed on one side by a 254-μm thin copper foil and on the other by a spring-loaded, Viton O-ring-sealed valve. Randomly distributed over our measurement period of 5 days we inserted a 19-mm-diam,

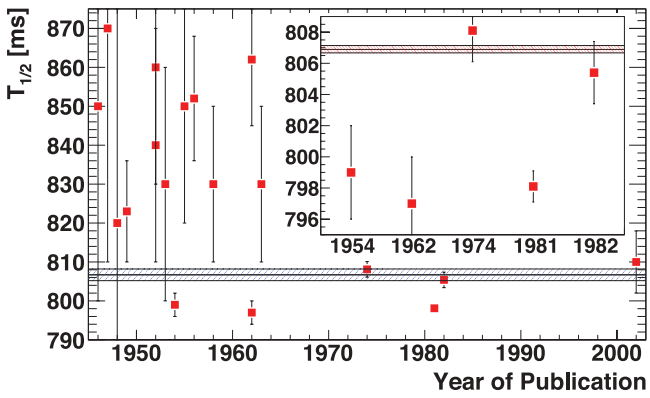

FIG. 1. (Color online) Compilation of the measured ^{6}He half-lives given in Table I. The dashed blue band shows the half-life adopted in Ref. [36] from the average of the two values found in Refs. [29,33] and used in compilations ever since. The inset shows the five values with uncertainties below 1% [23,29,31–33] with the dashed red band depicting the value for the ^{6}He half-life obtained in this paper.

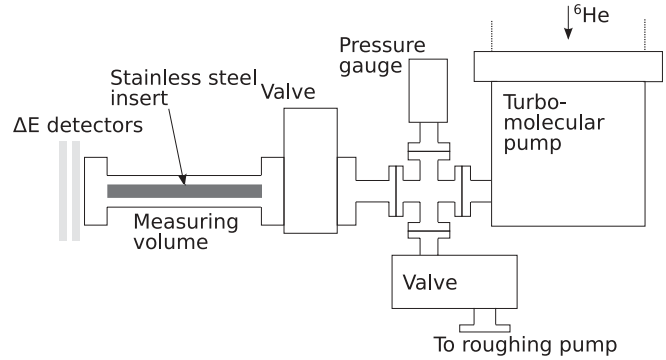

FIG. 2. Experimental setup with two thin scintillators placed in front of a measuring volume which can be closed off by a spring-loaded valve. The stainless steel insert was used to determine possible systematic effects due to diffusion of ^{6}He into the walls of the measuring volume.

283-mm-long stainless steel cylinder suspended in the center of the tube by four screws. With the stainless steel insert we increased the wall collision frequency of ^{6}He atoms by about 80% and used those data to check for possible diffusion of the ^{6}He atoms into the stainless steel surfaces. We took comparable amounts of data with and without this insert. Figure 2 shows a schematic drawing of the setup.

Directly in front of the measuring volume we placed two identical, 2.5-mm-thick plastic scintillators separated by 3.2 cm registering the βs from the decay of ^{6}He penetrating through the copper foil. The plastic scintillators were coupled via light guides to Hamamatsu photomultiplier tubes model R1450. Their output signals passed through timing filter amplifiers (Ortec model 474) providing ∼100-ns-long pulses with a ∼30-ns rise time. Two discriminators (LeCroy model 821) with thresholds right above the electronic noise provided the logic trigger signals. We formed the coincidence of those two signals resulting in a single 25-ns-long logic pulse. We passed this pulse through four gate generators (LeCroy model 222) providing signals of fixed, nonextendable dead times of lengths 1.9819(81), 3.9990(81), 6.0026(83), and 7.9758(83) μs. The details of the dead-time determination are given in Sec. IV. Subsequently, the four signals were fed into a CAMAC-based scaler (LeCroy model 2551) together with the original coincidence signal and the signals from a 1- and 100-kHz clock. The signal from the 1-kHz clock also triggered the readout of the scaler module via the software package JAM [39], thereby providing 1-ms time stamps to our data stream. The 100-kHz clock was used to detect potential scaler reading problems. These data were written to event files for offline analysis. A schematic of the whole electronics chain is shown in Fig. 3.

The timing sequence of the measurement was as follows: The data were acquired in 24-s-long measurement cycles. During a period of 8 s we directed the deuteron beam onto the lithium target and the outlet of the turbomolecular pump was connected to our measuring volume while the valve to the roughing pump was closed. For the following 16 s, thereby completing one cycle, we deflected the deuteron beam at the low-energy end of the accelerator, closed the spring-loaded

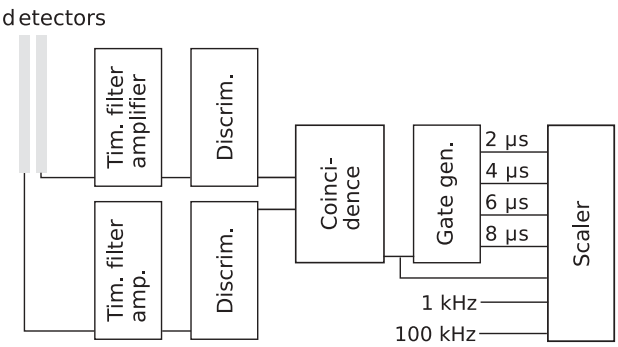

FIG. 3. Schematic of the electronics setup.

valve at the back of the measuring volume, and measured the ^{6}He half-life directly by observing the decay curve. At the same time the valve to the roughing pump opened and the ^{6}He exhaust was pumped away. During the last 100 ms of the 16-s decay time both valves were open in order to provide some pumping to the measuring volume.

With separate electronics, we performed pulse height measurements at the beginning of the measurements to determine our thresholds. We triggered the analog-to-digital converter (ADC) on the coincidence signal and took the pulse height spectra for both scintillators. Fitting the peak for the minimum ionizing particles we determined that ∼99% of the pulses (in each of the detectors separately) are above our threshold. The thresholds were estimated to be ∼30 keV based on the average energy deposition in the detector of ∼300 keV for a minimum ionizing particle.

III. DATA PROCESSING

We read the binary JAM files into ROOT [40] and created "raw histograms" with 1-ms bin size for each channel. At this stage, two main data defects could be detected: *missed readings* due to the data acquisition (DAQ) computer not reading out the scaler values and *incorrect readings* due to the scaler values updating while being read. Both of the defects were readily identified in the data stream. As the scaler retained the actual data unaffected by the missed and incorrect readings we were able to correct for them by distributing the counts of the next correct reading across the affected readings. From the raw histograms we created "differential histograms" for the different channels by calculating the differences between subsequent readings. The systematic uncertainties associated with this data correction are discussed in Sec. V.

To further reduce remaining data defects and improve the performance of the fitting at low statistics, we increased the bin size in the differential histograms to 10 ms. At the end we corrected for the dead-time losses on a cycle-by-cycle basis by calculating the true rate R_0 in each time bin from the measured rate R using the measured dead times τ_d: $R_0 = R/(1 - R\tau_d)$ [41]. Because we took data at different deuteron beam intensities to study decay-rate-dependent effects, the data are finally grouped into five different initial rate classes: <40, 40–50, 50–60, 60–70, and 70–80 kHz.

IV. DEAD-TIME MEASUREMENT

The dead time of the different channels was determined using the source and pulser method [42]. We placed a ^{90}Sr source in front of the two scintillators to act as the random source. The pulser was running at 10 kHz. The signals from the source and the pulser were merged at the stage of the long gate generator. In a first step, we measured the rate with the random source only. After 15–20 min of data acquisition, we read the total counts in each channel through the scaler. The total acquisition time was determined by a 10-Hz clock. In the next step, we performed the same measurement with the pulser on and determined the dead time by calculating [42]

$$\tau_d = \frac{1}{R_r}\left(1 - \sqrt{\frac{R_{pr} - R_r}{R_p}}\right), \tag{1}$$

where R_r is the rate of random signal, R_p is the rate of the pulser, and R_{pr} is the rate of the mixed signal.

The intrinsic dead time from the start of the detector pulses to the generation of the long gates was inspected with an oscilloscope. It amounted to ∼130 ns. As our long gates generated by the four gate generators were much longer than any preceding gates and signals, only the length of those four gates which we measured using the source and pulser method was relevant for the dead-time correction. Several dead-time measurements were performed following the ^{6}He decay data taking. The results of those runs were consistent with each other. We averaged the different runs resulting in the dead times 1.9819(81), 3.9990(81), 6.0026(83), and 7.9758(83) μs.

V. DATA ANALYSIS

Figure 4 shows the histogram for the full counting cycle for the data with initial rates <40 kHz, 2-μs dead time, and the stainless steel insert out. The step and wiggle right after 7.9 s is due to valve movement, when the valve of the decay volume is closed and the valve to the roughing pump is opened (we started the timing 100 ms after the beam turned on). It takes ∼200 ms for this effect to die out. In addition, because the systematic uncertainty due to the dead-time correction grows

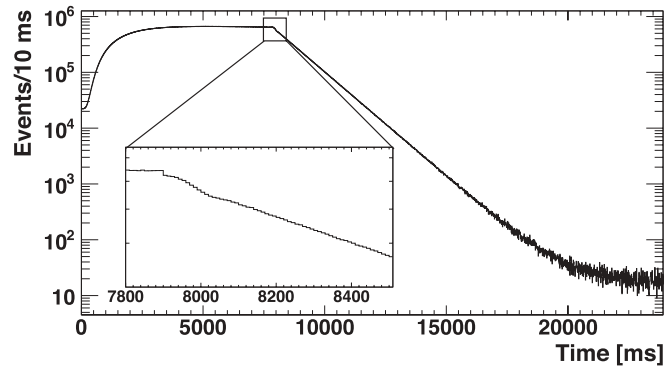

FIG. 4. Histogram for a full ^{6}He counting cycle for the data with initial rates <40 kHz and the stainless steel insert out. The insert zooms into the transition point from beam on to beam off at which the valve in front of the measuring volume closes and the valve to the roughing pump opens.

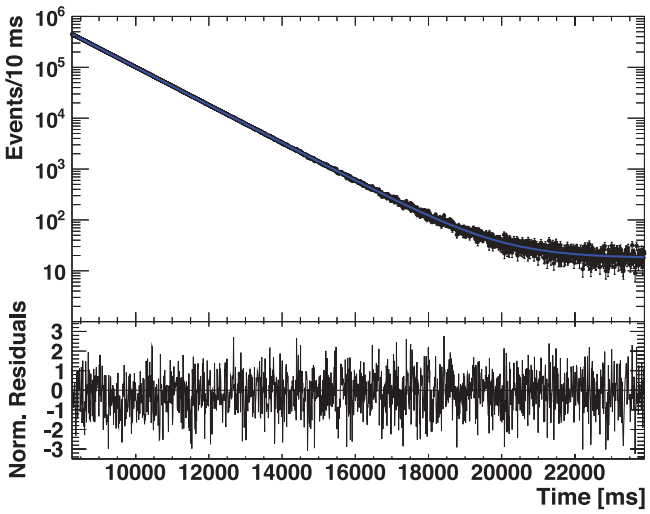

FIG. 5. (Color online) ^{6}He decay curve for the data with 2-μs dead time, initial rates <40 kHz and the stainless steel insert out with the corresponding residuals. The χ^2/DOF of the fit is 1578.2/1562.

rapidly with rate we delayed the starting point of our fit in each of the rate groups such that for the highest rate in that group the initial rate lies at 32 kHz. For the group with initial rates <40 kHz, the starting point is at 8260 ms—beyond the first 200 ms affected by the valve motion. The end point of the fit lies at 23 900 ms. The fit was performed using the modified χ^2 method outlined in Ref. [43]. Figure 5 shows the decay curve for the same data as in Fig. 4. Also shown is a fit to the function $f(t) = N\{\exp[-(t-t_0)/\tau] + b\}$, where the lifetime τ and the background b are free parameters while N is set by the normalization of the fitting function and the total counts of the histogram. The lower panel gives the corresponding residuals. We cross-checked our fit results, performing both regular χ^2 and maximum-likelihood fits. In addition, we performed the fits on simulated data consisting of $\sim 10^8$ random events distributed with a half-life of 807 ms and our measured background. Dead-time effects were applied to the time-ordered events and then corrected in the same manner as for our experimental data. The results of the different methods for both the experimental and simulated data are listed in Table II, showing their consistency and no particular bias.

Figure 6 shows a compilation of all the half-life fit results for the different rate groups and stainless steel insert in and out. The four different dead-time channels were combined,

TABLE II. ^{6}He half-life fitting results of the data shown in Fig. 5 and the simulated data using different methods. In our simple implementation of the maximum-likelihood fit the increased number of counts due to the dead-time correction are treated as an increase in statistics resulting in a slightly lower error with respect to the other methods.

Method	Expt. data (ms)	Simulated data (ms)
Modified χ^2	806.969 ± 0.114	807.019 ± 0.096
Regular χ^2	806.970 ± 0.114	807.025 ± 0.096
Max. likelihood	806.974 ± 0.113	807.023 ± 0.095

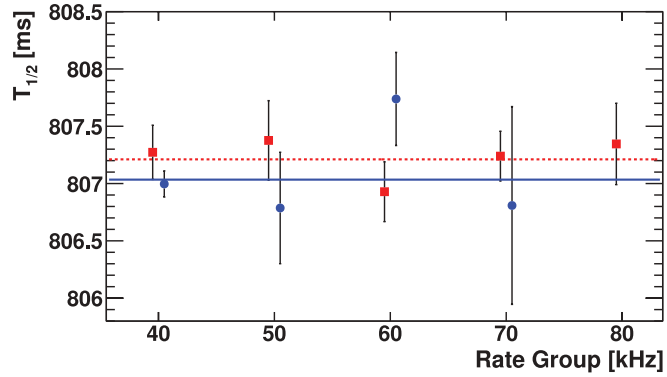

FIG. 6. (Color online) ^{6}He half-life fit results for the different rate groups with the initial rates restrained to 32 kHz. Only statistical errors are given. The squares (circles) correspond to the stainless steel insert in (out) data. The dashed (solid) line shows the constant fit to the insert in (out) data with χ^2/DOF of 1.6/4 (3.4/3). The results of the constant fits correspond to the averages given in Table III.

performing a weighted average and keeping the smallest of the statistical uncertainties. Table III gives the final results from the averages of the different rate groups. The individual dead-time channels were combined to yield the two average values for the two cases corresponding to the stainless steel insert in and out of the measuring volume. These two values are used below for an estimation of the potential diffusion of ^{6}He atoms into the stainless steel surfaces.

VI. SYSTEMATIC UNCERTAINTIES

In Table IV we give our estimates of systematic shifts and uncertainties that are described in detail in the following paragraphs. In several cases we used a simulation to determine the magnitude of the systematic uncertainty. The simulation consisted of generating $\sim 10^{10}$ (statistical uncertainty of 0.01 ms on the half-life) random events distributed with a half-life of 807 ms and our measured background. We then applied to the time-ordered events the different systematic effects and fit the data to determine the deviation from the input half-life.

TABLE III. List of the different ^{6}He half-lives obtained with various dead times and for the cases of the stainless steel insert in and out. The systematic shifts and uncertainties from Table IV are not included.

Insert	τ_d	Results (ms)	Average (ms)
Out	~2 μs	807.01 ± 0.11	807.03 ± 0.11
	~4 μs	807.03 ± 0.11	807.03 ± 0.11
	~6 μs	807.08 ± 0.11	807.03 ± 0.11
	~8 μs	807.02 ± 0.11	807.03 ± 0.11
In	~2 μs	807.20 ± 0.12	807.21 ± 0.12
	~4 μs	807.20 ± 0.12	807.21 ± 0.12
	~6 μs	807.21 ± 0.12	807.21 ± 0.12
	~8 μs	807.23 ± 0.12	807.21 ± 0.12

TABLE IV. List of systematic shifts and uncertainties for our ^{6}He half-life measurement. We added the errors in quadrature to obtain the total error. Where a second value is given it corresponds to the measurements with the stainless steel insert in.

Source	Shift (ms)	Uncertainty (ms)
Dead-time correction		0.04
Dead-time drift	0	0.009
^{6}He diffusion	0	$^{+0.12/+0.22}_{-0}$
Gain shift	−0.19	0.19
^{8}Li contamination	0	$^{+0}_{-0.007}$
Data correction	0	0.01
Afterpulsing	0	0.003
Clock accuracy	0.006	0.011
Background	0.046	0.004
Total	−0.14	$^{+0.23}_{-0.19}$ / $^{+0.29}_{-0.19}$

The effect of the dead-time correction is large. The correction shifts the half-life values by −9, −18, −27, and −35 ms for the four different dead-time channels, respectively. However, the agreement between the four values after the dead-time correction lends confidence to its validity. The results for the different dead-time channels are highly correlated and their differences should only be influenced by the corresponding loss in statistics, the uncertainty of which is given by $\sigma_{\text{corr}} = \sqrt{|\sigma_1^2 - \sigma_2^2|}$. Since our data for different dead-time channels are not completely correlated due to the data preselection, we modified the data preselection procedure to result in the exact same data set for all the dead-time channels. The results for this particular data set are shown in Table V, together with the differences between the 2-μs channel and the other channels and their corresponding error as calculated according to the description above. The differences are consistent with the loss of statistics in the different dead-time channels.

The uncertainty on the measured dead times of ∼8 ns translates directly into a systematic uncertainty on the half-life. Figure 7 shows the dependence of the fitted half-life values on changes in the dead time as determined from data. The linear slope of −0.00485 ms/ns results in a systematic uncertainty of 0.04 ms. Although a small and constant spread in the fixed dead times does not introduce any systematic uncertainty, a drift in the dead times obviously does. We tracked the length of the 2-μs gate during 7 days on a digital oscilloscope. Although we observed variations of ±2 ns on a daily basis there

TABLE V. List of the different ^{6}He half-lives obtained with the completely correlated data in four dead-time channels for the case of the stainless steel insert out. The differences and corresponding errors are given with respect to the 2-μs channel.

Insert	τ_d	Results (ms)	Diff. (ms)	σ_{corr} (ms)
Out	∼2 μs	806.999 ± 0.169		
	∼4 μs	806.992 ± 0.170	− 0.007	0.017
	∼6 μs	807.000 ± 0.171	0.001	0.025
	∼8 μs	806.963 ± 0.172	− 0.036	0.030

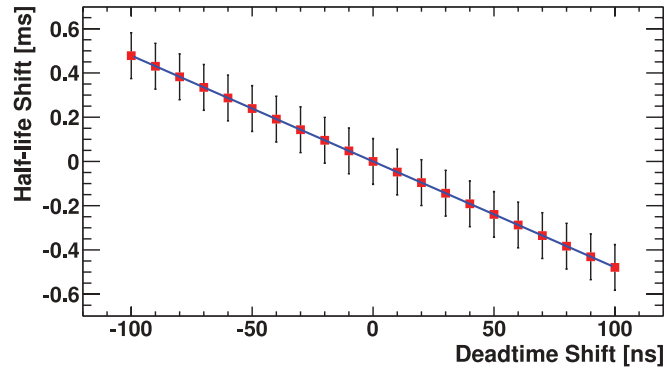

FIG. 7. (Color online) Shifts in the fitted ^{6}He half-life values as a function of changes in the dead time used in the dead-time correction. The data correspond to the averages of the different dead-time channels. The slope amounts to −0.00485 ms/ns.

was no long-term drift detectable. We attribute a systematic uncertainty of 0.009 ms in the half-life to these observed drifts.

Using a helium leak detector we studied the diffusion of helium through the walls of the measuring volume and the Viton O-ring of the valve at its end. While we did not observe any diffusion through the walls, we did observe the diffusion of helium atoms through the valve O-ring. Figure 8 shows the resulting helium gas flow into the leak detector with one side of the closed valve connected to its inlet and the other side filled to 1 atm of helium. In our analysis we follow Refs. [44–46]. We found acceptable agreement between our data and the predicted gas flow $C(t)$ as given in Eq. (46) of Ref. [44],

$$C(t) = C_0\left[1 + 2\sum_{n=1}^{\infty}(-1)^n \exp\left(-(n\pi)^2\frac{Dt}{d^2}\right)\right], \quad (2)$$

for a diffusivity $D = 10^{-5}$ cm^2/s and a steady-state flow $C_0 = 5.7 \times 10^{-8}$ mbar l/s. The thickness d of the O-ring in the valve

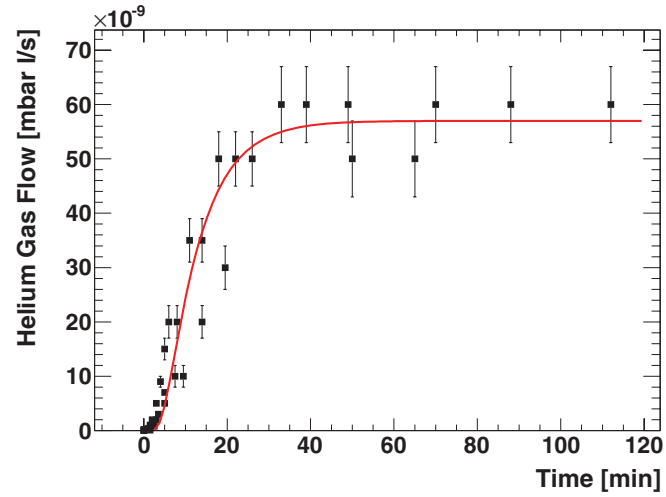

FIG. 8. (Color online) Measured helium leak rates through the Viton O-ring of the valve sealing our measurement volume. The plot compiles three separate measurements. The line shows the prediction for the gas flow according to Eq. (46) of Ref. [44] for a diffusivity $D = 10^{-5}$ cm^2/s and a steady-state flow $C_0 = 5.7 \times 10^{-8}$ mbar l/s.

was measured to be 2.2 mm. There is an uncertainty of about a factor of 2 in the extracted diffusivity due to the thickness and about 20% on the steady-state flow due to the sensitivity of the leak detector. From these two measurements we extract a permeability $K = 10^{-10}$ (cm^3 at STP) mm s^{-1} mbar^{-1} cm^{-2} using an exposed area of $A = 1.2$ cm^2 and a solid solubility $b = 10^{-6}$ (cm^3 at STP) mbar^{-1} cm^{-3} for helium in the Viton O-ring of our valve. Both of these values are in acceptable agreement with values found in the literature. We neglect any mass scaling of the measured flow by $\sqrt{m_{^4\mathrm{He}}/m_{^6\mathrm{He}}}$ and an exponentially decreased diffusivity because of the higher mass. During our cycle length of $T = 16$ s the ^{6}He atoms diffuse a distance $l \sim 2\sqrt{DT}$ into the O-ring, resulting in an absorbed gas volume $V_{\mathrm{gas}} = 2\sqrt{DT}Abp_{^6\mathrm{He}}$ at the ^{6}He partial pressure $p_{^6\mathrm{He}}$. The average loss rate over the full cycle thus amounts to

$$\frac{1}{T}\frac{N_{\mathrm{loss}}}{N_0} = \frac{1}{T}p_0 b\frac{2\sqrt{DT}A}{V_0} = 5\times 10^{-9}\ \mathrm{s}^{-1} \qquad (3)$$

with $p_0 = 1000$ mbar, the total number of ^{6}He atoms N_0, and the volume of our measuring volume $V_0 = 367$ cm^3. This represents a negligible shift at our precision.

Although we were not able to observe any diffusion through the walls of the measuring volume, we assume that some diffusion does occur, leading to an additional loss channel. The mean free path $\lambda = 4V/A$ inside our measuring volume V and surface area A leads to a wall-collision frequency $f_c = v/\lambda$ given the velocity v of the atoms. Any time constant $1/\tau_{\mathrm{diff}}$ associated with this loss channel scales linearly with the wall-collision frequency $f_c = v/\lambda$ and leads to a measured lifetime $1/\tau = 1/\tau_{^6\mathrm{He}} + 1/\tau_{\mathrm{diff}}$. From the absence of any significant difference between the two results listed in Table III we conclude that $\tau_{\mathrm{diff}} \gg \tau_{^6\mathrm{He}}$ and the difference between the two results is $\Delta(1/\tau) = 1/\tau_{\mathrm{in}} - 1/\tau_{\mathrm{out}} = (-2.8 \pm 2.5)\times 10^{-7}$ ms^{-1} $= 0.8/\tau_{\mathrm{diff}}$ where the factor 0.8 is due to the 80% increased wall-collision frequency with the insert in place. We set the Gaussian probability density function to zero in the nonphysical region [37] and calculate an upper limit on $1/\tau_{\mathrm{diff}}$ at a 68% confidence limit (C.L.) of 2×10^{-7} ms^{-1}. This translates into a systematic uncertainty for the insert in and out data of $^{+0.22}_{-0}$ and $^{+0.12}_{-0}$ ms, respectively.

Examining our highest rate data, we identified traces of a small, rate-dependent shift, which is not fully accounted for by our dead-time correction. Though pileup effects could potentially be the cause of such a shift, based on the arguments given below its effect is too small to contribute. Therefore, because the values are shifted toward higher half-life values, we attribute it to a negative decrease in gain with increased rate in the photomultiplier tubes. For a potential reduction in gain of 10% a fraction of 10^{-3} of the counts falls below threshold as determined from the pulse-height measurements performed at the beginning of the data taking. This would lead to a systematic shift of the half-life of 0.16 ms as obtained from our simulations and gives the approximate order of magnitude of such potential gain shifts. To investigate the size of the rate-dependent shift from our data constrained to 32 kHz itself, we added a parameter k to our fitting function to model the effect of a linear rate dependence by substituting in our fitting function $R(t) \to R(t)[1 - kR(t)]$. The resulting shift in the half-life

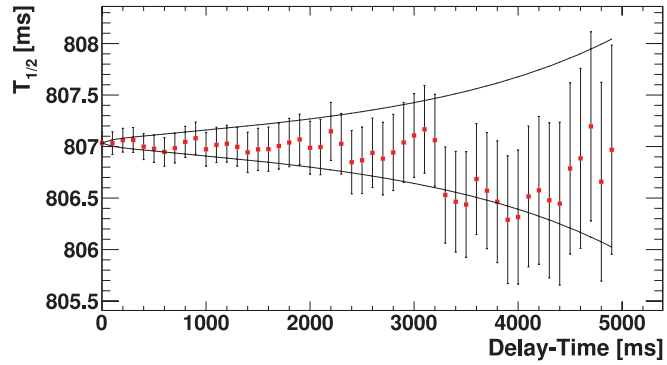

FIG. 9. (Color online) ^{6}He half-life values as a function of delay in the starting point of the fits. The two solid lines correspond to the $\pm 1\sigma$ contours for the allowed variation (relative to the first data point) that one expects from the loss in statistics for this correlated data set.

due to including the parameter k amounts to -0.19 ± 0.19 ms, showing no significant rate-dependent effect after corrections. We did not observe any difference in this shift between the two data sets with the stainless steel insert in or out. As a consistency check, we also examined our data by plotting the fit results as a function of start time shown in Fig. 9. Because the start time of the fit is different in each of the rate groups the values are given as a function of "delay time" corresponding to the delay of the start time in each rate group. The two solid lines on that plot correspond to the $\pm 1\sigma$ contours given by the loss in statistics for this correlated data set. The data around the rather large drop at about 3 s was studied in more detail in search of a potential artifact but we concluded there is no anomaly.

A potential contaminant in our system—apart from tritium, which cannot influence our measurement—is the β emitter ^{8}Li ($t_{1/2} = 838.40(36)$ ms, β^- decay with end point 16.0 MeV [47,48]) produced by the reaction ^{7}Li(^{2}H,^{1}H)^{8}Li. The Li atoms are not expected to reach our counting station but rather get trapped in the Li target or in the walls during the many collisions ($\sim 10^5$) that occur before atoms can reach the detection area. Nevertheless, in separate measurements using both of our two thin scintillators used for the half-life measurements but also a thick scintillator to measure the full energy of the β particles, we scanned the deuteron beam energy below the ^{7}Li(^{2}H,^{3}He)^{6}He reaction threshold of 5.8 MeV, but above the one for ^{8}Li of 0.25 MeV [48]. Although we still observed a small production rate of a β emitter, both the energy spectrum with an end point of 3.5 MeV and the extracted half-life of 810 ± 5 ms clearly identify it as ^{6}He. The observed production agrees with a rough estimate of it being produced by the reaction ^{6}Li(n,^{1}H)^{6}He where the neutrons are produced via ^{7}Li(^{2}H,n). Integrating the background-subtracted β-energy spectrum above the ^{6}He end point and operating at our nominal deuteron beam energy we set an upper limit of 2×10^{-4} at 68% C.L. on the fraction of possible ^{8}Li contamination translating to a systematic uncertainty of 0.007 ms.

Throughout the data taking we performed several background runs in which we kept the valve in front of the measuring volume closed but otherwise operated the experiment just like for the other runs. Our background runs are distributed

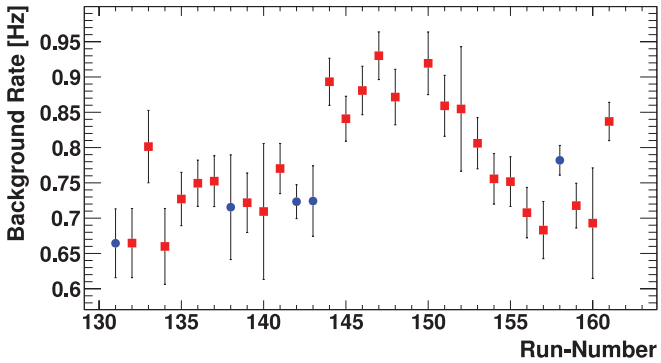

FIG. 10. (Color online) Measured background rates during dedicated background runs (blue circles) and fitted background rates in half-life data taking runs (red squares).

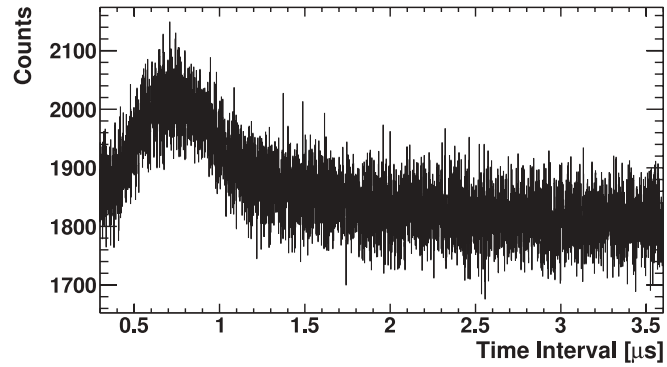

FIG. 11. Histogram of the time between two events as measured with a time-to-amplitude converter in the range 0–4 μs. We see a clear indication of spurious afterpulses at 0.75 μs.

across all of the lifetime data and largely average out the changes in background levels or deuteron beam current. While we initially saw a significant contribution stemming from ^{6}He β particles penetrating through the thin-walled stainless steel bellows of our roughing pump, we were able to greatly reduce that background by shielding the bellows with lead. The data taken before this provision were not included in the analysis. The measured background rate in background runs and the fitted background rate in half-life data taking runs are shown in Fig. 10. The average background rate of the data taking runs was 0.8 ± 0.1 Hz, which is consistent with the average of the rates of the background runs. Combining all the background run data after shielding the bellows, we still observed a small decay structure with a half-life of 507(27) ms and an amplitude of 6.3(3) times the value of the constant background in the background runs. Although this is most probably still coming from ^{6}He that is being pumped away, it could also be the result of some beam-related activation. Regardless of its origin, we studied this time-dependent background by including it in the fitting function $R(t) = N(\exp[-(t-t_0)/\tau] + b\{1 + A\exp[-(t-t_0)/\tau_b]\})$, where A is the ratio of the amplitude of the extra decay structure and the background and τ_b is the lifetime of the extra decay structure. We assumed that A was the same in the half-life data taking runs as that in the background runs. By varying A and τ_b in the range measured in the background runs, we concluded that the extra decay structure results in a systematic shift of 0.046 ms with an uncertainty of 0.004 ms.

We studied our data-correction procedure outlined in Sec. III in detail using the simulation with the occurrences of the different defects determined from the data. We did not observe any significant shift within the statistical uncertainty of the simulation. We also performed our fits on the data without any data corrections, resulting in a consistent value. We thus attribute a systematic uncertainty of 0.01 ms (the statistical uncertainty of our simulation) to our data-correction procedure.

In a dedicated effort we measured the time distribution between two consecutive coincidence events using a time-to-amplitude converter to search for spurious afterpulses owing to electronic or instrumental effects. We found an excess of events in the 4-μs full range setting leading to a 0.7-μs-wide peak at 0.75 μs sitting on top of an otherwise perfectly exponential behavior [41] shown in Fig. 11. The probability of occurrence of those excess events is 3×10^{-4}. Although we are protected from those excess events by the dead times, we performed a simulation with such an excess centered at 3.5 μs to study its potential influence. Table VI lists the results of that simulation with the differences and associated uncertainty calculated as in the discussion on dead time above. There is a small effect visible in the 2-μs channel. As a conservative estimate of the systematic uncertainty, we use the statistical uncertainty of the simulation of 0.01 ms. The afterpulse height is about four times the noise amplitude in Fig. 11, so the systematic uncertainty for a frequency of occurrence at the detection limit in the spectrum is 0.003 ms.

We measured the precision of our 1-kHz clock by comparing the summed number of ticks over 16 days with respect to the time provided by NIST [49]. The accumulated difference amounts to -11 ± 1 s over a period of 1.37×10^6 s, which corresponds to a shift of -8.03 ± 0.73 ppm. Owing to potential changes in temperature, we assign an additional 13.35 ppm to the frequency uncertainty. Therefore, we estimated the systematic shift and uncertainty to be 0.006 ± 0.011 ms.

Pileup effects do not play a significant role in our measurement because of our long dead times and low threshold. One way that pileup would influence our result is if two coinciding pulses below threshold result in a pulse above threshold. As given in Sec. II, the threshold cuts away ~1% of the electron spectrum in each scintillator. The probability of two pulses of length $\tau_p \approx 100$ ns coinciding at a given rate R is given by $R\tau_p$. The probability that those two pulses are below threshold is $P_{\text{pile}} = 10^{-4}$. The correction that would need to be

TABLE VI. Obtained ^{6}He half-life values in our afterpulse simulation. The differences and corresponding uncertainties are with respect to the 8-μs channel.

Channel	Fitted half-life (ms)	Diff. (ms)	σ_{corr} (ms)
~2 μs	806.99984 ± 0.00957	0.0078	0.0020
~4 μs	806.99348 ± 0.00964	0.0014	0.0016
~6 μs	806.99331 ± 0.00971	0.0012	0.0011
~8 μs	806.99209 ± 0.00977		

applied to the data thus takes the form $R_0 = R(1 - P_{\text{pile}} R\tau_p)$ in order to obtain the true rate R_0 given the measured rate R. Combined with the dead-time correction, the final correction (neglecting higher-order infinitesimals) looks like $R_0 \approx R/[1 - R(\tau_d - P_{\text{pile}}\tau_p)]$. Therefore, this pileup effect behaves like a ∼0.01-ns correction to the dead time, which leads to a negligible shift in our half-life value of 5×10^{-5} ms. Another effect of pileup would stem from the coincidence of two pulses directly at the end of the long dead-time gate, which would thus not free the trigger at the appropriate time and would extend the dead time. However, this requires the coincidence of three pulses, the probability of which is given by $(R\tau_p)^2$ corresponding to $\sim 10^{-5}$ at our highest rates. At the highest rates this leads to an extension of the dead time by a negligible 0.001 ns. Owing to both effects being negligible we do not list them in Table IV.

VII. RESULTS

Because the result of our measurements with the stainless steel insert is dominated by the systematic uncertainty owing to a potential diffusion of the ^{6}He atoms into the surface we do not average the two values given in Table III. We report the data from our measurements without the insert as our final result, yielding a ^{6}He half-life of

$$T_{1/2} = 806.89 \pm 0.11_{\text{stat}}{}^{+0.23}_{-0.19\,\text{syst}}\ \text{ms}, \tag{4}$$

where the first error is statistical and the second systematic. From this, we proceed to determine the ft value for the β decay of ^{6}He and extract the corresponding Gamow-Teller matrix element. We calculated the Q value of the decay to be 3.505208(53) MeV/c^2 using the recent ^{6}He mass determination obtained in a Penning trap [50] and the value for ^{6}Li [51]. This corresponds to a 4σ shift compared to previously reported values [52]. The relation between the ft value and the Gamow-Teller matrix element M_{GT} is

$$f^\star t(1 + \delta'_R)(1 + \delta_{\text{NS}} - \delta_C) = \frac{K}{G_V^2\left(1 + \Delta_R^V\right) g_A^2 |M_{\text{GT}}|^2} \tag{5}$$

following the definitions and notation of Ref. [53]. We set the parameters δ_{NS} and δ_C to zero—or equivalently absorb them into the definition of M_{GT}—and calculated the radiative correction δ'_R to be 1.0365(13)%. We adopted the value for the parameters $K/[G_V^2(1 + \Delta_R^V)] = 6143.62 \pm 1.66$ s from the world average of superallowed $0^+ \to 0^+$ nuclear β decays [53]. The statistical rate function is given by $f^\star = \int F(Z, E) pE(E - E_0)^2 f_1(E) dE = f(1 + \delta_s)$, where f is the value of the integral in the absence of the shape-correction function $f_1(E)$ and δ_s is the correction to it when including $f_1(E)$. Here $F(Z, E)$ is the Fermi function, p and E the electron momentum and energy, and E_0 the end-point energy. We obtain $f = 995.224(68)$ yielding an ft value of $803.04^{+0.26}_{-0.23}$ s, where we added the statistical and systematic errors in quadrature. To take into account the shape correction, we performed shell-model calculations using the Cohen-Kurath interaction [54] and with the Warburton-Brown interaction, denoted PWBT in Ref. [55], adjusted to reproduce either the experimental Gamow-Teller matrix element or the weak magnetism term, which in Holstein's notation [56] is $b = 68.4(7)$, determined from the width of the $0^+ \to 1^+$ transition in ^{6}Li [57]. Both adjustments result in almost identical terms for the statistical rate function and we obtain $f^\star = 997.12(58)$. From this we calculate the experimental value for the Gamow-Teller matrix element in ^{6}He β decay as $|M_{\text{GT}}| = 2.7491(10)/|g_A|$. Using $g_A = -1.2701(25)$ [37] determined from the decay of the free neutron, we get $|M_{\text{GT}}| = 2.1645(43)$.

VIII. COMPARISON WITH THEORY

Given the precision obtained in our measurement it is worthwhile to itemize the improvements (both experimental and theoretical) that affect the extraction of the Gamow-Teller matrix element, M_{GT}. Table VII lists the shifts that have occurred in M_{GT} arising from (a) an improvement in the Q-value determination, (b) an improvement in the calculation of the nucleus-dependent radiative correction, and (c) the inclusion or not of the shape-correction function in the statistical rate function calculation. The benchmark experimental ft value used by theorists [4,13–15] up until now dates back to Ref. [58] and a statistical rate function obtained from the tabulated values of Wilkinson and Macefield [59]. By happenstance our half-life measurement agrees with the value adopted in Ref. [36] so no shifts owing to a revision in the half-life are included in Table VII. First, the improvement in the Q-value measurement leads to a 0.26% shift in the value of the Gamow-Teller matrix element. Second, the tabulated values of the statistical rate function of Wilkinson and Macefield include the radiative correction calculated to order α. Today, it is normal to extend these calculations to order $Z\alpha^2$ and $Z^2\alpha^3$; see, for example, Ref. [60]. These extensions give a small shift in M_{GT} of 0.03%. Third, the inclusion of a shape-correction function induces a small −0.09% shift. That this shift is so small in ^{6}He β decay is a reflection of the fact that this transition is very fast and the "allowed" approximation of ignoring the spectrum shape works very well. In more retarded transitions this correction would become more significant. The sum of these three shifts is quite small, producing an experimental M_{GT} value that is in agreement, within errors, of the one used previously in comparisons with theory. However, the extraction of the experimental Gamow-Teller matrix element given here stands on a more solid footing.

To make comparisons on the possible quenching of g_A we define an experimental axial coupling constant for ^{6}He, $g_A^{^6\text{He}}$,

TABLE VII. List of shifts in the determination of the experimental Gamow-Teller matrix element.

Source	Shift in $f^\star$	Shift in $\lvert M_{\text{GT}}\rvert$
Shift in Q value[a]	−0.51(10)%	0.26(5)%
Improved radiative correction		0.0299(6)%
Shape factor δ_s	0.19(6)%	−0.09(4)%

[a]Shift owing to the recent mass measurement of ^{6}He with $\Delta Q/Q = -0.086\%$ [50].

TABLE VIII. Comparison between the experimental Gamow-Teller matrix element obtained in this work and the various calculations. As our measurement determines the product $|g_A|M_{GT}$ we present the comparison with theory by calculating $|g_A^{^6He}| = |g_A|M_{GT}/M_{GT}^{calc}$ and comparing it to the value for the axial coupling constant obtained from free neutron decay $g_A = -1.2701(25)$ [37]. LO stands for "leading order" and MEC for "meson-exchange currents." Where two values are given they represent the results of different calculations by changing, e.g., the wave functions (Ψ_T) or nuclear potentials (AV8′, TM′(99)) used. For the exact details on those changes and the calculations we refer to the provided references.

	Matrix element M_{GT}^{calc}					
Ref.	M_{GT} (LO)		M_{GT} (incl. MEC)		$\lvert g_A^{^6He}\rvert$	$(\lvert g_A^{^6He}\rvert - \lvert g_A\rvert)/\lvert g_A\rvert$
[13]	2.254(5)	(Ψ_T I)	2.284(5)	(Ψ_T I)	1.204	− 5.2%
	2.246(10)	(Ψ_T II)	2.278(10)	(Ψ_T II)	1.207	− 5.0%
[4]	2.283	(AV8′+TM′(99))			1.204	− 5.2%
	2.305	(AV8′)			1.193	− 6.1%
[14]	2.157(1)	(Ψ_T I GFMC)			1.275	0.4%
	2.207(3)	(Ψ_T II GFMC)			1.246	− 1.9%
[15]	2.225(2)		2.198(7)		1.251	− 1.5%
This work	$\lvert g_A\rvert M_{GT} = 2.7491(10)$					

as

$$\left|g_A^{^6He}\right| = \frac{1}{M_{GT}^{calc}}\sqrt{\frac{K}{G_V^2\left(1+\Delta_R^V\right)f^{\star}t(1+\delta_R')(1+\delta_{NS}-\delta_C)}} = \frac{|g_A|M_{GT}}{M_{GT}^{calc}} \quad (6)$$

using the calculated matrix elements M_{GT}^{calc}. Table VIII shows the comparison for the matrix elements between our experimental result and the different calculations and the experimental axial coupling constant for ^{6}He and the one obtained from the free neutron. The two most recent calculations are off by about 1.5%, with older calculations showing a difference of ∼5%. Clearly the need for a large quenching of g_A as observed in shell-model calculations of *sd*-shell nuclei is not needed here. Only Ref. [4] gives the calculated width of the analogous $M1$ transition in excellent agreement to within the experimental uncertainty of 2%. Interesting measurements to complement our result would be improved determinations of the $M1$ width and of the muon capture rate on ^{6}Li [61] to a precision of $\lesssim$1%. The latter would directly test a possible momentum-transfer dependence of the effective weak axial coupling in nuclei [12].

IX. CONCLUSIONS AND SUMMARY

We performed the most precise measurement of the ^{6}He half-life of $806.89 \pm 0.11_{stat}{}^{+0.23}_{-0.19\,syst}$ ms, thereby improving the precision over the currently reported value [36] by a factor of 6. Our result is in good agreement with two of the previous five values [29,33] with precisions of less than 1% but deviates from the three others by up to 8.6σ [23,31,32]. Because the possibility of diffusion out of the target was not directly addressed in these experiments we speculate that this may be the cause of the discrepancy. Calculating the statistical rate function we determined the ft value to be $803.04^{+0.26}_{-0.23}$ s. The extracted Gamow-Teller matrix element of $|M_{GT}| = 2.1645(43)$ agrees within a few percent with *ab initio* calculations using the weak axial coupling constant g_A measured in free neutron decay. Our precise determination allows for improved comparisons between theory and experiment and may allow using ^{6}He in addition to ^{3}H to fix low-energy constants in the effective-field-theory description of the electroweak processes.

ACKNOWLEDGMENTS

We thank the excellent staff at the Center for Experimental Nuclear Physics and Astrophysics. Fruitful discussions with Smarajit Triambak are gratefully acknowledged. We thank Wick Haxton and Bob Wiringa for helpful comments. This work has been supported by the U.S. Department of Energy under Grant No. DE-FG02-97ER41020. P.M. and W.W. acknowledge support by the Department of Energy, Office of Nuclear Physics, under Contract No. DEAC02-06CH11357.

[1] K. Kubodera and M. Rho, in *From Nuclei to Stars, Festschrift in Honor of Gerald E. Brown*, edited by S. Lee (World Scientific, Singapore, 2011).
[2] S. C. Pieper and R. B. Wiringa, Annu. Rev. Nucl. Part. Sci. **51**, 53 (2001).
[3] P. F. Bedaque and U. van Kolck, Annu. Rev. Nucl. Part. Sci. **52**, 339 (2002).
[4] P. Navrátil and W. E. Ormand, Phys. Rev. C **68**, 034305 (2003).
[5] B. A. Brown and B. H. Wildenthal, At. Data Nucl. Data Tables **33**, 347 (1985).
[6] W.-T. Chou, E. K. Warburton, and B. A. Brown, Phys. Rev. C **47**, 163 (1993).
[7] F. Osterfeld, Rev. Mod. Phys. **64**, 491 (1992).

[8] J. Rapaport and E. Sugarbaker, Annu. Rev. Nucl. Part. Sci. **44**, 109 (1994).
[9] E. Caurier, A. Poves, and A. P. Zuker, Phys. Rev. Lett. **74**, 1517 (1995).
[10] W. C. Haxton and C.-L. Song, Phys. Rev. Lett. **84**, 5484 (2000).
[11] I. S. Towner, Phys. Rep. **155**, 263 (1987).
[12] J. Menéndez, D. Gazit, and A. Schwenk, Phys. Rev. Lett. **107**, 062501 (2011).
[13] R. Schiavilla and R. B. Wiringa, Phys. Rev. C **65**, 054302 (2002).
[14] M. Pervin, S. C. Pieper, and R. B. Wiringa, Phys. Rev. C **76**, 064319 (2007).
[15] S. Vaintraub, N. Barnea, and D. Gazit, Phys. Rev. C **79**, 065501 (2009).
[16] A. Knecht *et al*., Phys. Rev. Lett. **108**, 122502 (2012).
[17] R. Raabe *et al*., Phys. Rev. C **80**, 054307 (2009).
[18] H. S. Sommers and R. Sherr, Phys. Rev. **69**, 21 (1946).
[19] Veeraraghavan, Proc. Indian Acad. Sci. **43** A, 319 (1956).
[20] J. M. Cassels and R. Latham, Nature (London) **159**, 367 (1947).
[21] W. B. Herrmannsfeldt, R. L. Burman, P. Stähelin, J. S. Allen, and T. H. Braid, Phys. Rev. Lett. **1**, 61 (1958).
[22] W. J. Knox, Phys. Rev. **74**, 1192 (1948).
[23] J. K. Bienlein and F. Pleasonton, Nucl. Phys. **37**, 529 (1962).
[24] J. E. R. Holmes, Proc. Phys. Soc. (London) A **62**, 293 (1949).
[25] S. Malmskog and J. Konijn, Nucl. Phys. **38**, 196 (1962).
[26] R. K. Sheline, Phys. Rev. **87**, 557 (1952).
[27] J. B. Vise and B. M. Rustad, Phys. Rev. **132**, 2573 (1963).
[28] Vendryes, Ph.D. dissertation, University of Paris, 1952 (unpublished).
[29] D. H. Wilkinson and D. E. Alburger, Phys. Rev. C **10**, 1993 (1974).
[30] M. E. Battat and F. L. Ribe, Phys. Rev. **89**, 80 (1953).
[31] P. H. Barker, T. B. Ko, and M. J. Scandle, Nucl. Phys. A **372**, 45 (1981).
[32] R. M. Kline and D. J. Zaffarano, Phys. Rev. **96**, 1620 (1954).
[33] D. E. Alburger, Phys. Rev. C **26**, 252 (1982).
[34] B. M. Rustad and S. L. Ruby, Phys. Rev. **97**, 991 (1955).
[35] D. Anthony, L. Buchmann, P. Bergbusch, J. M. D'Auria, M. Dombsky, U. Giesen, K. P. Jackson, J. D. King, J. Powell, and F. C. Barker, Phys. Rev. C **65**, 034310 (2002).
[36] F. Ajzenberg-Selove, Nucl. Phys. A **413**, 1 (1984).
[37] K. Nakamura *et al*. (Particle Data Group), J. Phys. G **37**, 075021 (2010).
[38] A. Knecht *et al*., Nucl. Instrum. Methods Phys. Res., Sect. A **660**, 43 (2011).
[39] K. B. Swartz, D. W. Visser, and J. M. Baris, Nucl. Instrum. Methods A **463**, 354 (2001).
[40] ROOT Data Analysis Framework, http://root.cern.ch/drupal/
[41] G. F. Knoll, *Radiation Detection and Measurement* (Wiley, New York, 2000).
[42] A. P. Baerg, Metrologia **1**, 131 (1965).
[43] G. F. Grinyer *et al*., Phys. Rev. C **71**, 044309 (2005).
[44] R. M. Barrer, *Diffusion in and Through Solids* (Cambridge University Press, Cambridge, 1941).
[45] P. Sturm, M. Leuenberger, C. Sirignano, R. E. M. Neubert, H. A. J. Meijer, R. Langenfelds, W. A. Brand, and Y. Tohjima, J. Geophys. Res. **109**, D04309 (2004).
[46] S. J. Schowalter, C. B. Connolly, and J. M. Doyle, Nucl. Instrum. Methods Phys. Res., Sect. A **615**, 267 (2010).
[47] X. Fléchard *et al*., Phys. Rev. C **82**, 027309 (2010).
[48] National Nuclear Data Center (NNDC), http://www.nndc.bnl.gov
[49] National Institute of Standards and Technology (NIST), http://nist.time.gov
[50] M. Brodeur *et al*., Phys. Rev. Lett. **108**, 052504 (2012).
[51] B. J. Mount, M. Redshaw, and E. G. Myers, Phys. Rev. A **82**, 042513 (2010).
[52] G. Audi, A. Wapstra, and C. Thibault, Nucl. Phys. A **729**, 337 (2003).
[53] J. C. Hardy and I. S. Towner, Phys. Rev. C **79**, 055502 (2009).
[54] S. Cohen and D. Kurath, Nucl. Phys. **73**, 1 (1965).
[55] E. K. Warburton and B. A. Brown, Phys. Rev. C **46**, 923 (1992).
[56] B. R. Holstein, Rev. Mod. Phys. **46**, 789 (1974).
[57] TUNL Nuclear Data Evaluation Project, http://www.tunl.duke.edu/nucldata/
[58] F. Ajzenberg-Selove, Nucl. Phys. A **320**, 1 (1979).
[59] D. H. Wilkinson and B. E. F. Macefield, Nucl. Phys. A **232**, 58 (1974).
[60] I. S. Towner and J. C. Hardy, Phys. Rev. C **77**, 025501 (2008).
[61] J. P. Deutsch *et al*., Phys. Lett. B **26**, 315 (1968).